Attenuation of multifrequency laser radiation along extended atmospheric paths

A.A. Zemlyanov, Yu.V. Kistenev, V.V. Kolosov, Yu.N. Ponomarev, and K.M. Firsov

Institute of Atmospheric Optics,
Siberian Branch of the Russian Academy of Sciences, Tomsk

Received March 15, 2000

The estimates of absorption of CO, HF, and DF lasers multifrequency radiation along extended atmospheric paths are presented in the paper. Peculiarities in the behavior of absorption characteristics depending on the path profile, spectrum of the laser emission, and meteorological conditions are analyzed. We also analyze the influence of thermal nonlinearity on the beam characteristics.

Introduction

Application of lasers with the emission spectra comprising many lines to multifrequency sensing of gas and aerosol composition of the atmosphere opens new possibilities as compared with those based on the frequency-tunable narrow-band lasers. In this paper the estimates of molecular absorption of a wide-band laser radiation are presented and some peculiarities in the transfer of such a radiation along horizontal and slant atmospheric paths are described.

Diatomic molecular systems like CO, HF, and DF have enjoyed the widest application in wide-band gas lasers. They provide for high power of output radiation both in cw and pulsed modes of operation. The emissions of these lasers have line spectra that depend on the mode of pumping, composition and working temperature of a mixture, geometry of cavity, the presence of selective elements, and so on. Therefore, there exist a great variety of similar lasers with strongly different characteristics. We used, in our calculations, the values of parameters for typical CO, HF, and DF lasers described in the literature.[1–4]

Basov et al.[2] have studied experimentally the evolution in time of the total rotational-vibrational structure of the radiation spectrum of pulsed cryogenic electroionization CO laser with wide-band nonselective cavity, operating in the free-running lasing. The generation at 15 vibrational bands has been obtained. The radiation spectrum of such a laser has many (up to 10) vibrational bands, and their number increases with the increasing pump. The spectral and energy characteristics of a cw CO laser built up using a commercially available LG–22–CO device are presented in Ref. 3. The CO laser emission spectrum with nonselective cavity consisted of 36 lines in the vibrational bands $v \to v - 1$ from $19 \to 18$ to $7 \to 6$ in the range from 1626 to 1914 cm^{-1} (Fig. 1). The radiation spectra of HF and DF lasers also consist of a large number of lines. Figures 2 and 3 show their emission spectra observed experimentally. The data for simulation were borrowed from Ref. 4.

In Ref. 5 simultaneous emission of more than two hundred lines has been obtained in the range from 2.6 to 3.2 μm by frequency conversion of radiation of a low pressure CO laser using a $ZnGeP_2$ crystal. Since a noncritical phase matching occurred, in doubling the five-micron radiation in the nonlinear crystal, the second harmonics generation and summation of individual frequencies from the entire emission spectrum took place almost simultaneously. This effect was taken into account in simulating cw and pulsed CO laser emission spectra within the range of 2.6–2.9 μm. In the case of lasers with CO and HF active media, the simulation took into account the second harmonics generation.

The emission spectra of the lasers considered partly coincide with rather strong absorption bands of water vapor and CO_2, where total attenuation of radiation can take place at a distance of several centimeters. The CO laser emission is within a strong 6.3 μm absorption band of H_2O (Fig. 1). Figures 2 and 3 depict the atmospheric absorption spectra in the ranges 2.7–3.3 and 3.7–4.9 μm, where the 2.7 μm absorption band of water vapor and 4.3 μm absorption band of CO_2 are located.

Model of calculation of wide-band radiation transmission

The selective absorption by H_2O, CO_2, O_3, N_2, and other molecules, as well as the scattering by microparticles in suspension are the main processes that accompany propagation of the IR radiation through the atmosphere.

A peculiarity of the atmospheric molecular absorption is its strong spectral variability (the typical values of the absorption line halfwidths vary from 10^{-3} to 10^{-1} cm^{-1}). Relatively small variations of laser generation frequency (to ~1 cm^{-1}) may result in the absorption coefficient change over several orders of magnitude. Thus, for example, the values of absorption coefficients within the H_2O absorption bands in the ground layer under typical summer conditions may reach 10^4 km^{-1} and more, whereas in the transmission microwindows the radiation can propagate at sufficiently large distances. In this connection, for an adequate estimation of the atmospheric transmission for a particular laser, comprehensive information on its emission spectrum is needed. In particular, the emission line frequency ought to be known accurate to better than 0.01 cm^{-1}.

0235-6880/00/05 463-09 $02.00

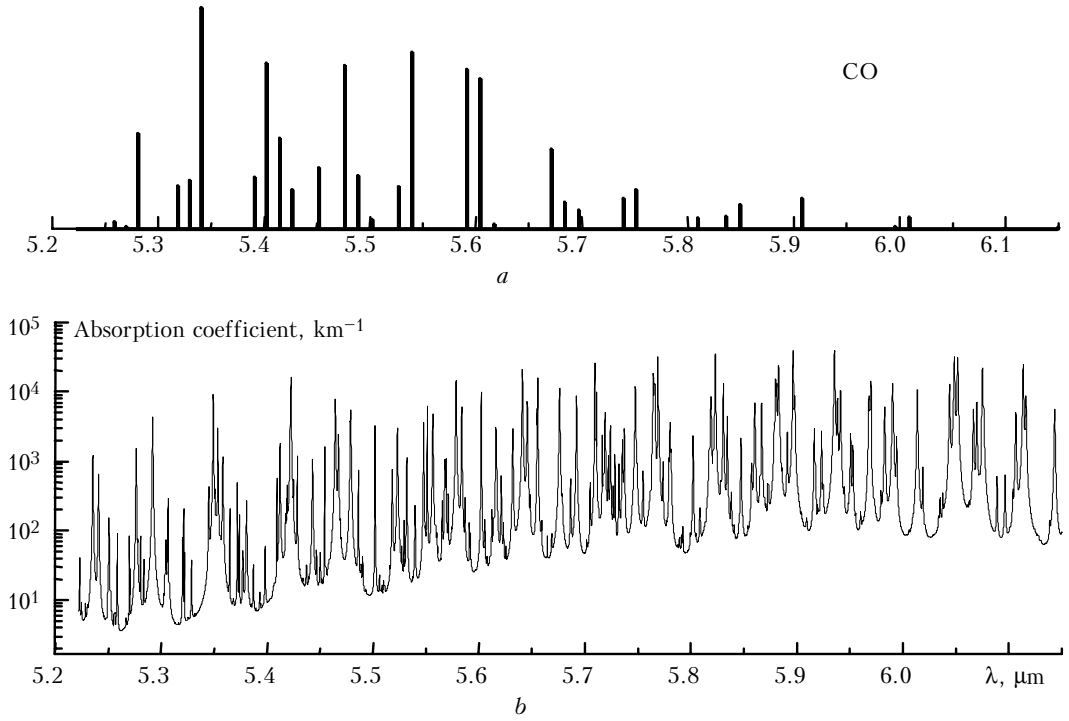

Fig. 1. Spectral distribution of a cw CO laser radiation energy (*a*); absorption spectrum of the atmosphere in the ground layer (*b*).

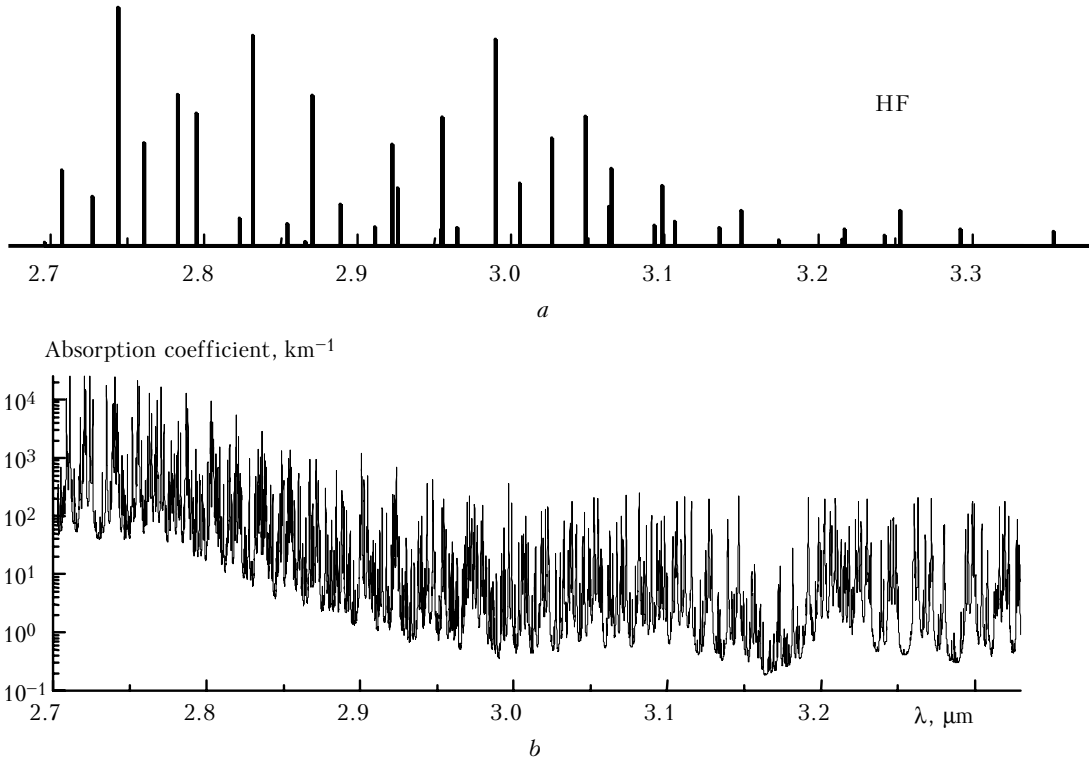

Fig. 2. Spectral distribution of HF laser radiation energy (*a*); atmospheric absorption spectrum in the ground layer (*b*).

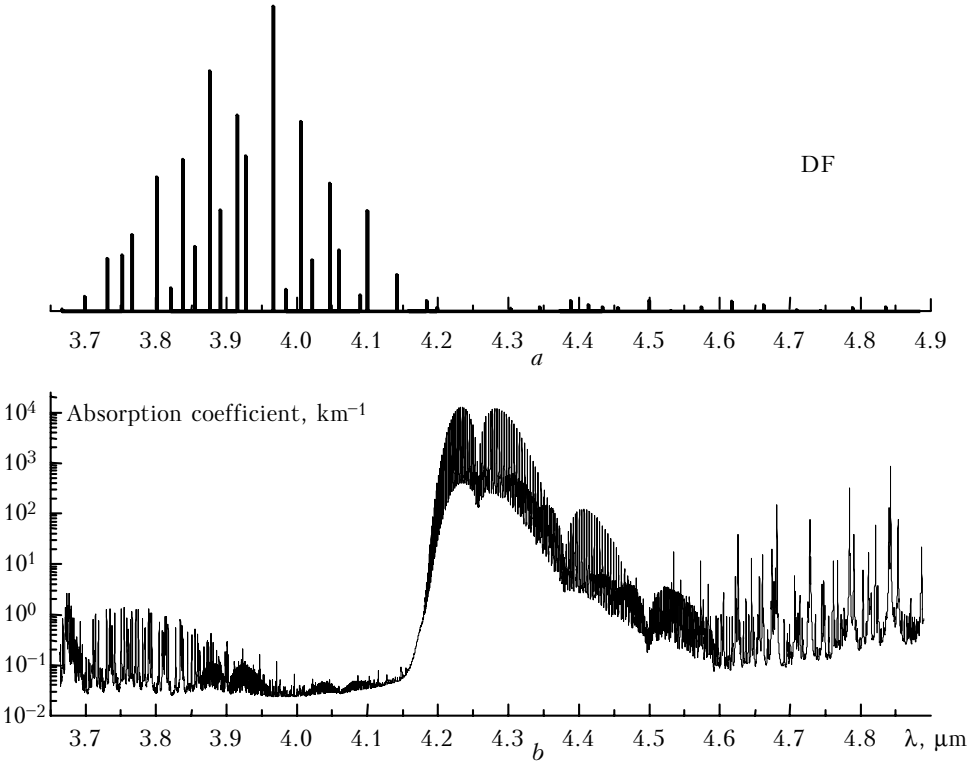

Fig. 3. Spectral distribution of DF laser radiation energy (*a*); atmospheric absorption spectrum in the ground layer (*b*).

One more peculiarity of the molecular absorption coefficient is in its strong altitude dependence. The concentration of gases (particularly of H_2O) rapidly falls off with the increasing height. Besides, as the air pressure decreases, the number of molecular collisions also decreases, what results in line shape narrowing. Therewith, the strongest altitude changes in the absorption coefficient take place in the transparency microwindows.

The molecular absorption coefficients have been calculated using a version of the direct line-by-line method,[6,7] designed by the authors, and data from the HITRAN–96 spectral database (see Ref. 8). For atmospheric transmission macro- and microwindows, where far wings of spectral absorption lines play a significant part, a noticeable difference between the experimental data and those calculated with the use of the Lorentz contour can appear. Therefore, the continual absorption in these spectral ranges was taken into account based on the model described in Ref. 9.

In our calculations, we modeled the Earth's atmosphere as spherically layered medium, with the parameters altered in accordance with the models of standard atmosphere.[10] The attenuation of laser radiation due to molecular absorption was computed by the following formula:

$$T = \sum_{i=1}^{n} I_i \exp\left\{-\int_0^L \alpha_i[h(l)]\,\mathrm{d}l\right\} \Big/ \sum_{i=1}^{n} I_i; \qquad (1)$$

$$h(l) = \sqrt{(R + z_1)^2 + l^2 + 2l(R + z_1)\sin\theta} - R, \qquad (2)$$

where I_i is the intensity of the ith laser radiation line, L is the path length, θ is the path zenith angle, z_1 is the source altitude, R is the Earth's radius (R = 6380 km), and $\alpha_i(h)$ is the molecular absorption coefficient (km^{-1}) at the altitude h.

Formula (1) was derived ignoring the ray trajectory variation due to refraction and assuming incoherent radiation.

Relative variation of the path length in some homogeneous atmospheric layer due to refraction at its boundary with the preceding one can be estimated as

$$\delta h / h \approx -\,\delta\theta\,\tan\theta,$$

where $d\theta$ is the difference between the angles of refraction and incidence at the layers boundary. Taking into account Snellius law, we can write

$$\delta h / h \approx \delta n\,\tan^2\theta, \qquad (3)$$

where δn is the refractive index variation at the boundary between layers. For plane-stratified medium the estimate of relative variation of the path length can be written as

$$\delta L / L \approx (n_0 - 1)\,\tan^2\theta, \qquad (4)$$

where n_0 is the refractive index in the ground atmospheric layer. Note, that the magnitude of $(n_0 - 1)$ is, as a rule, of the order of 10^{-4} (Ref. 11).

It is known (see, for example, Ref. 12) that the pulse length significantly increasing the time of the medium phase relaxation $\tau = 1/\gamma_{ij}(h)$ complies with the conditions of incoherent interaction. This time is about $\tau \sim 10^{-9}$ s in the ground atmospheric layer. As the path altitude in our calculations did not exceed 30 km, it follows that the model (4) applies in the cases of pulse duration much longer than 10^{-7} s.

Calculated results

We have calculated atmospheric transmission along various paths in trying to reveal general regularities in propagation of the above laser emissions through the atmosphere.

The calculated results are given in Tables 1–4. As is seen from the tables, the CO laser radiation experiences most strong attenuation, because its emission spectrum falls in the strong H_2O absorption band. Therefore, the attenuation by the Earth's atmosphere in summer time is essentially stronger than in winter (see Tables 1, 2). Note that the second harmonic radiation also falls in the water vapor absorption band in 2.7 μm region. The transmittance of a horizontal path rapidly grows as the path altitude increases because of a decrease in water vapor content thus decreasing the absorption.

Table 1. Atmospheric transmission for CO laser radiation along the paths of different lengths

h_1, km	h_2, km	L, km	Transmission, %			
			Pulsed CO laser		Continuous wave CO laser	
			summer	winter	summer	winter
0	0	1	0.44	6.42	0.08	1.90
	10	10	0.02	1.58	0	0.36
	25	25	0.02	1.55	0	0.36
	30	30	0.02	1.55	0	0.35
3	10	300	0	0	0	0
	15	300	0	0	0	0
	25	300	0	0.01	0	0
	10	500	0	0	0	0
	15	500	0	0	0	0
	25	500	0	0	0	0
10	10	300	0.23	18.17	0.04	10.68
	30	300	61.13	86.75	43.83	79.32
	10	500	0	0	0	0
	30	500	24.03	66.74	13.98	51.92
	87.8	1000	22.55	65.70	13.03	50.76
15	15	300	86.91	89.79	80.71	86.11
	30	300	96.33	96.61	95.44	95.89
	15	500	11.10	51.44	6.09	37.07
	30	500	92.31	92.95	89.39	90.63
	92.7	1000	93.94	94.42	91.87	92.78
25	30	300	98.25	98.41	97.89	98.08
	30	500	96.91	97.18	95.76	96.16
	25	300	97.85	98.02	97.18	97.39
	25	500	96.19	96.45	94.68	95.10
	102.6	1000	98.47	98.61	98.24	98.41

Note. h_1 is the path's altitude above the ground at the beginning of the path; h_2 is the altitude of a radiation detector at the end of the path; L is the path's length.

Table 2. Atmospheric transmission for CO laser radiation (second harmonic) along the paths of different lengths

h_1, km	h_2, km	L, km	Transmission, %			
			Pulsed CO laser		Continuous wave CO laser	
			summer	winter	summer	winter
0	0	1	0	0	0	0
	10	10	0	0	0	0
	25	25	0	0	0	0
	30	30	0	0	0	0
3	10	300	0	0	0	0
	15	300	0	0	0	0
	25	300	0	0	0	0
	10	500	0	0	0	0
	15	500	0	0	0	0
	25	500	0	0	0	0
10	10	300	0	0	0	0.02
	30	300	0.23	1.57	4.44	13.77
	10	500	0	0	0	0
	30	500	0	0.32	0.10	5.32
	87.8	1000	0	0.29	0.08	5.07
15	15	300	0.97	1.37	13.31	15.57
	30	300	8.18	10.62	25.57	26.84
	15	500	0	0.08	0	2.37
	30	500	1.83	2.54	18.67	19.72
	92.7	1000	2.92	4.07	21.01	22.06
25	30	300	41.18	45.53	43.53	46.86
	30	500	20.08	24.13	30.83	33.26
	25	300	29.88	34.01	36.46	39.33
	25	500	10.45	13.38	26.51	28.02
	102.6	1000	45.64	49.89	46.63	49.89

The HF lasers radiation in one or other degree, depending on the emission spectral range, falls into the strong 2.7 μm absorption band of water vapor (see Table 3). Figure 2 presents the atmospheric absorption spectrum in this spectral region for the atmospheric ground layer under climate conditions of mid latitude summer. The result was obtained by direct calculation using the information from the HITRAN–96 database. As is seen, the long wave spectral portion of the HF laser emission is at the band's periphery and is attenuated by the atmosphere to a lesser degree than the CO laser radiation. Nevertheless, the HF laser radiation is almost completely absorbed along extended atmospheric paths (we used in our calculations the path lengths up to 300–500 km), passing wholly or in part through the ground layer. Only when the entire path is at an altitude, where the water vapor is practically absent (10 km and higher), the fraction of radiation passed through is close to or exceeds 50%.

The calculated results on the atmospheric transmission for DF laser radiation are presented in Table 4. The atmospheric absorption for this laser radiation is essentially lower than for the above-mentioned lasers. This can be explained by the fact that the main portion of DF laser radiation spectrum is in the atmospheric transmission window in the 3 to 5 μm region. The atmospheric absorption of radiation in this spectral region is caused by the wings of absorption bands of such main atmospheric gases as water vapor and CO_2. The weaker bands of methane also contribute

to the absorption in this region. It should be noted that absorption of this laser radiation also strongly depends on the path altitude.

Table 3. Atmospheric transmission for HF laser radiation along the paths of different lengths

h_1, km	h_2, km	L, km	Transmission, %			
			Fundamental frequency		Second harmonic	
			summer	winter	summer	winter
0	0	1	14.65	23.32	44.43	55.14
	10	10	9.21	17.23	37.36	48.00
	25	25	9.12	17.09	37.16	47.79
	30	30	9.11	17.08	37.13	47.76
3	10	300	0.01	0.72	18.36	23.29
	15	300	0.20	3.17	21.98	28.17
	25	300	1.94	7.97	27.01	35.51
	10	500	0	0	8.02	13.61
	15	500	0	0.01	13.68	17.86
	25	500	0.03	1.32	19.50	24.84
10	10	300	10.38	25.58	40.64	63.66
	30	300	43.88	56.35	83.50	94.79
	10	500	0.17	3.27	21.80	28.61
	30	500	28.06	44.49	66.50	86.32
	87.8	1000	27.50	44.00	65.77	85.87
15	15	300	52.83	55.54	95.01	96.18
	30	300	63.62	64.82	98.59	98.70
	15	500	22.15	37.30	59.35	79.77
	30	500	57.23	59.01	97.24	97.52
	92.7	1000	59.56	61.17	97.83	98.04
25	30	300	71.61	73.87	99.16	99.21
	30	500	66.24	67.47	98.87	98.97
	25	300	68.67	70.07	99.06	99.12
	25	500	63.78	65.00	98.64	98.76
	102.6	1000	73.06	75.83	99.21	99.25

Table 4. Atmospheric transmission for DF laser radiation along the paths of different lengths

h_1, km	h_2, km	L, km	Transmission, %	
			summer	winter
0	0	1	93.66	95.24
0	10	10	86.35	88.68
0	25	25	85.62	87.94
0	30	30	85.61	87.93
3	10	300	28.65	35.82
3	15	300	42.67	47.40
3	25	300	57.66	60.31
3	10	500	1.46	6.72
3	15	500	10.11	18.57
3	25	500	33.07	39.06
10	10	300	63.60	62.78
10	30	300	84.30	84.20
10	10	500	36.71	37.45
10	30	500	73.80	73.27
10	87.8	1000	73.45	72.90
15	15	300	80.01	79.62
15	30	300	92.24	92.23
15	15	500	67.04	65.99
15	30	500	84.65	84.31
15	92.7	1000	87.57	87.35
25	30	300	97.34	97.47
25	30	500	95.49	95.53
25	25	300	96.58	96.65
25	25	500	93.38	93.33
25	102.6	1000	97.58	97.72

The absorptance of a molecular medium for radiation propagating through it is one of its most important characteristics in many practical applications. The absorptance for a monochromatic radiation is determined by the molecular absorption coefficient. The volume absorption coefficient is solely determined by the local thermodynamic parameters of the atmosphere. It decreases as the altitude increases and does not depend on the direction of radiation propagation.

However, the volume absorption coefficient for a multifrequency radiation cannot be recorded directly, at least without a frequency selection. Therefore, the measure of the medium absorptance in this case is the quantity

$$A(L) = - \mathrm{d} \ln T / \mathrm{d}L, \qquad (5)$$

which naturally appears, for example, in interpreting the data obtained using a differential absorption method.

In contrast to the absorption coefficient, the parameter $A(L)$ is not a local characteristic of a medium. Below we shall term this quantity as the effective molecular absorptance.

Figure 4 presents the values of $A(L)$ calculated for HF laser radiation propagated along two types of vertical atmospheric paths. At upward propagation, the absorption coefficient $A(L)$ rapidly decreases with height. At the downward propagation, the altitude behavior of $A(L)$ has quite different character. The difference between the coefficients reaches two orders of magnitude. In the second case the altitude dependence of $A(L)$ is rather nontrivial: it not only slightly varies with the height, but also begins to grow at large altitudes. Thus, the magnitude of $A(L)$ turns to be dependent on the direction of propagation, although the nonlinear phenomena capable of causing this effect,[13] are not considered here.

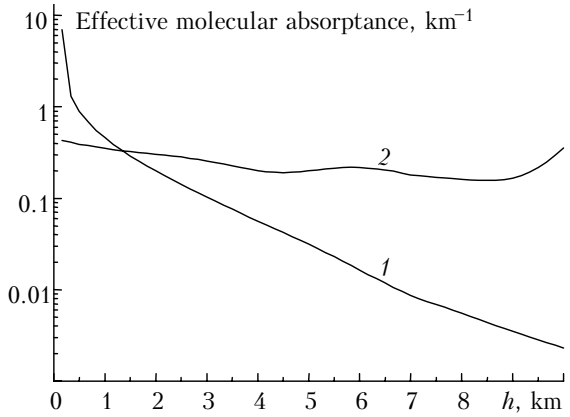

Fig. 4. Vertical profile of the effective molecular absorptance of the atmosphere for HF laser multifrequency radiation: (*1*) upward propagation (0–10 km), (*2*) downward propagation (10–0 km). The meteorological model of the mid-latitude summer was used in calculations.

To better explain such a behavior of $A(L)$, we have performed calculations for a homogeneous near-ground path, in this case the volume absorption

coefficients $\alpha_i(h)$ are constant (Fig. 5). It is seen from Fig. 5 that $A(l)$ has a pronounced maximum in the beginning of the path, then slowly decreases down to a saturation level. To qualitatively interpret the results obtained, it is reasonable to use the simplest model, in which the intensities I_i of all lines in the laser radiation spectrum are equal. We also assume that at some wavelengths λ_k the values of the absorption coefficient α_k are much lower than those at all other frequencies. In this case, after some elementary transformations formula (5) takes the form

$$\frac{\sum\limits_{i=1\ i\neq k}^{n} \alpha_i \exp\left[-(\alpha_i - \alpha_k) L\right] + \alpha_k}{\sum\limits_{i=1\ i\neq k}^{n} \exp\left[-(\alpha_i - \alpha_k) L\right] + 1}.$$

$$\text{At } L \to 0 \quad A = \frac{1}{n}\sum_{i=1}^{n} \alpha_i, \text{ and at } L \to \infty \quad A = \alpha_k.$$

The latter relations show that the strongest lines of molecular absorption contribute to the effective molecular absorptance primarily in the beginning of the path. In the process of propagation, laser radiation, within the strong bands of atmospheric absorption, is almost completely attenuated in the very beginning of the path. As a result, only those lines remain in the radiation spectrum, for which the coefficients of losses are comparatively small, and at the path's far end the effective molecular absorptance becomes a constant, which is equal to the minimum absorption coefficient. Thus, in the case of a homogeneous path, the maximum absorption of such a radiation occurs in the beginning of the path while being minimum one in its end.

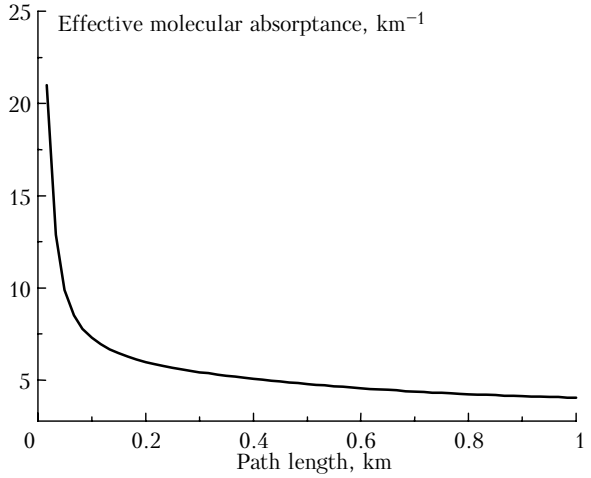

Fig. 5. Dependence of the effective molecular absorptance for HF laser multifrequency radiation on spatial coordinate at propagation along a homogeneous near-ground path of 1 km length. The meteorological model of the mid-latitude summer was used in calculations.

To study the general regularities in $A(L)$ behavior along the extended atmospheric paths, we have made calculations for three types of lasers under the same atmospheric conditions. We have chosen a tangential path of 500 km length with the initial and final points at the altitudes of 10 km. The CO laser radiation is absorbed almost totally, the transmission for HF laser radiation is about 0.1%, and the absorption for DF laser radiation is a bit higher than 60%. Analysis of the model results, presented in Fig. 6, shows that the behavior of the effective molecular absorptance for a wideband radiation is mainly determined by the overlap of laser radiation spectrum with the spectrum of atmospheric absorption. Noticeable difference in the $A(L)$ altitude behavior for HF laser is due to more uniform distribution of the emission lines of this laser over the atmospheric absorption band, i.e., a portion of it falls in the center of the H_2O absorption band at 2.7 μm with the other lines being in its periphery.

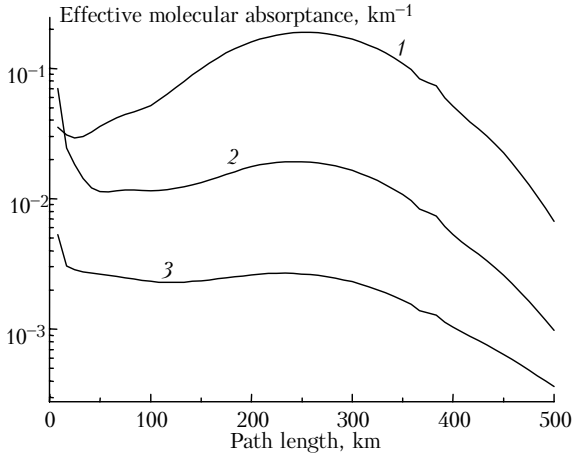

Fig. 6. Dependence of the effective molecular absorptance on spatial coordinate along a tangentian path of 500 km length (the path's beginning and end points are at altitudes of 10 km, the minimum altitude is 5.1 km). The meteorological model of mid-latitude summer was used. (*1*) CO laser, (*2*) HF laser, (*3*) DF laser.

Propagation of radiation along extended atmospheric paths

The above features of absorption of multifrequency laser radiation essentially influence the nonresonance nonlinear effects as the high-power beams propagate through the atmosphere. The thermal blooming of continuous and quasi-continuous wave (repetitively pulsed) radiation has the lowest threshold.[14,15] It manifests itself in an increase in the air temperature due to absorption of a portion of beam energy and, consequently, in variation of the dielectric constant of the medium, which becomes inhomogeneous across the beam. This results in the beam thermal distortions at its propagation, as well as in the wave phase distortions, which are different at different points of the beam and cause redistribution of the energy in it. The medium heating at electromagnetic energy dissipation into heat

is accompanied by relaxation processes (cooling) due to the wind transfer, convection, heat conductivity, and beam scanning.

Mathematically, the problem of thermal nonlinear optics can be reduced to analysis of equations of wave propagation and thermodynamics.[11,14,15] In this paper, we study the propagation of continuous (quasi-continuous) laser beam. In this case, the thermal blooming goes on in so-called regime of stationary "wind" nonlinearity.

The calculations of beam propagation under conditions of thermal blooming were conducted based on the radiation transfer equation

$$\left[\frac{\partial}{\partial z} + \iota \nabla_R + \frac{1}{2} \nabla_R \varepsilon(z, \mathbf{R}) \nabla_\iota\right] J(z, \mathbf{R}, \iota) = 0 , \quad (6)$$

where $J(z, \mathbf{R}, \iota)$ is the brightness introduced as the Fourier-transform of the coherence function

$$\Gamma_2(z, \mathbf{R}, \rho) = k^2 \iint_{-\infty}^{\infty} J(z, \mathbf{R}, \iota) \exp(i k \iota\rho) \, d^2\iota. \quad (7)$$

This is the first order equation. Traditionally, it can be solved by the method of characteristics. The Gaussian approximation of the brightness function over angular coordinate allows one to reduce the partial differential equation (6) to the system of ordinary differential equations, which assumes constructing the efficient numerical algorithms.[16–18]

The calculations are performed for the radiation source and receiver set aboard airplanes, the characteristic transverse speed of which (relative to the path direction) was 100 m/s. The results are obtained for various atmospheric paths, the parameters of which are listed in Table 5.

Table 5

Path's number	h_1, km	h_2, km	L, km	α, degs
1	10	10	500	−2.2
2	10	30	500	0
3	15	15	300	−1.3
4	15	30	300	1.8
5	15	3	500	−3.6

Note: α is the elevation angle of the path, other designations being the same as in Table 1.

Table 6 presents the parameters of lasers, for which the calculations have been made. The initial distribution of radiation intensity is assumed to be Gaussian with 1 m radius at the intensity level e^{-1}; the radiation power density is 30 W/cm^2; the initial radiation divergence two times exceeds the diffraction limit, i.e., we deal with a partially coherent radiation with transverse radius of spatial coherence, equal to approximately one half of the beam radius. The radiation is focused in the receiving plane. Table 6 also lists the mean wavelengths for these multifrequency lasers.

Table 7 presents the calculated results for the efficient power density W_{ef}, the efficient beam radius R_{ef}, and the diffraction limited value of the beam radius R_{dif} (found taking into account partial coherence) in the receiving plane. The values of these parameters were calculated by the following formula

$$W_{ef} = P/S_{ef}; \quad (8)$$

$$S_{ef}(z = L) = \pi R_{ef}^2;$$

$$R_{ef}^2 = \frac{1}{P(z = L)} \iint_{-\infty}^{\infty} (R^2 - R_c^2) W(\mathbf{R}, z = L) \, d^2\mathbf{R} , \quad (9)$$

$$\mathbf{R}_c(z = L) = \frac{1}{P(z = L)} \iint_{-\infty}^{\infty} \mathbf{R} \, W(\mathbf{R}, z = L) \, d^2\mathbf{R},$$

$$R_{dif}^2 = (1 - z/F)^2 + \frac{z^2}{k^2 R_0^4} + \frac{z^2}{k^2 r_c^4} , \quad (10)$$

where P is the radiation power in the receiving plane, S_{ef} is the beam efficient area, W is the radiation intensity, R_0 is the initial beam radius, r_c is the transverse radius of the radiation coherence, and F is the focal length.

The high-altitude extended paths are heterogeneous due to altitude variation above the Earth's surface along the path. The single-frequency radiation is mostly absorbed at the path's legs close to the surface. Such legs may be at any part of the path depending on the elevation angle of a slant path. Thus, for paths No. 1 and No. 3 the minimum height was just in the paths' middle, for the paths No. 2 and No. 4 – in their beginning, and for the path No. 5 – in its end. Physically, it is evident that at equal total absorption along the path, more strong distortions take place in the path's beginning as compared with its middle or the far end, because an approach of nonlinear lens to the radiation source increases its distorting action, whereas the defocusing action of the lens located in the path's end has no time to manifest itself.

Table 6

Laser number	Laser type	Harmonic	Mode of operation	Wavelength, μm	Beam divergence, rad	Type of resonator
1	HF	Second	Quasi-cw	1.35	$0.430 \cdot 10^{-6}$	nonselective
2	HF	fundamental	Quasi-cw	2.75	$0.876 \cdot 10^{-6}$	nonselective
3	CO	Second	cw	2.75	$0.876 \cdot 10^{-6}$	selective
4	DF	fundamental	Quasi-cw	4.3	$1.370 \cdot 10^{-6}$	nonselective
5	CO	fundamental	Quasi-cw	5.1	$1.623 \cdot 10^{-6}$	selective

Nonetheless, as it follows from the results presented in Table 7, noticeable nonlinear distortions are seen for the path No. 5 for all types of lasers. This is explained by the above peculiarity in the absorption of multifrequency laser radiation along the atmospheric paths due to the extraction of the major part of radiation energy in the beginning of the path. Thus, only 8 of 86% of total radiation losses of the HF laser second harmonic radiation (laser No. 1) are experienced by the beam at the second part of the path No. 5. The maximum loss is observed at the distance about 100 km from the source, i.e., in the path's first quarter. It is obvious that such an approach of nonlinear lens to the source essentially increases its distorting action.

Table 7

Path's number	Laser number	Transmission	W_{ef}, W/cm^2	R_{ef}, m	R_{dif}, m
1	1	0.2179	17.2	0.64	0.215
1	2	0.0017	0.06	0.94	0.438
1	3	0.0152	0.63	0.88	0.438
1	4	0.3660	16.3	0.85	0.685
1	5	0.0001	0.001	1.19	0.812
2	1	0.6650	159	0.36	0.215
2	2	0.2806	14.6	0.78	0.438
2	3	0.7780	102	0.49	0.438
2	4	0.7380	43.1	0.74	0.685
2	5	0.8858	41.3	0.82	0.812
3	1	0.9497	1572	0.14	0.129
3	2	0.5273	118	0.38	0.263
3	3	0.8822	342	0.28	0.263
3	4	0.7988	130	0.44	0.411
3	5	0.9900	133	0.49	0.487
4	1	0.9859	1863	0.13	0.129
4	2	0.6361	171	0.34	0.263
4	3	0.9469	415	0.27	0.263
4	4	0.9224	168	0.42	0.411
4	5	0.9830	130	0.49	0.487
5	1	0.1368	9.3	0.68	0.215
5	2	0.0000	0	0.92	0.438
5	3	0.0001	0	0.92	0.438
5	4	0.1010	3.9	0.90	0.685
5	5	0	0.00	1.24	0.812

The peculiarities in molecular absorption of multifrequency high-power laser radiation along extended atmospheric paths give rise to more essential differences. A characteristic manifestation of nonlinear thermal effects is that they limit a possibility of concentrating radiation in the receiving plane.[14,15] This manifests itself in the fact that as the source power increases, the radiation power density in the receiver plane grows up to some limiting value and then begins to lower, i.e., there exists some optimum value of the initial power, at which the maximum W_{ef} can be reached.

Another peculiarity of the nonlinear propagation of radiation through a medium is that nonlinear perturbations of the refractive index of a medium result in additional distortions of the beam phase. Therefore, the focusing of radiation on the receiving plane becomes less optimal from the viewpoint of maximum energy concentration in this plane. It is characteristic of a homogeneous distribution of the absorption coefficient along the path that the optimum distance of focusing exceeds the path length, i.e., radiation is focused beyond the receiving plane. This changes the position of the beam caustic (minimum cross section), where maximum concentration of radiation energy, and, consequently, maximum manifestation of nonlinear effects take place.[15]

For heterogeneous paths with nonlinear layer adjacent to the radiation source, the optimum focusing is located closer to the receiving plane. Sharper focusing is needed to compensate for the defocusing action of this nonlinear lens, because the caustic located at the path's end, where the nonlinearity is absent, does not exhibit its effect. The cases, when the maximum nonlinear effects are observed in the middle of the path or in its end, are close to that of homogeneous path, and the focusing is made, as the rule, beyond the receiving plane. Therefore, for single-frequency radiation and extended atmospheric paths with the elevation angle α equal to or greater than zero, the focusing is chosen to be closer to the receiving plane, whereas for the paths, where the receiver and the source are at the same altitude or the receiver is lower, the focusing is made beyond the receiving plane.

Table 8 presents the computations aimed at optimizing the initial power and focusing of a multifrequency laser radiation. Column 3 lists the initial power values at which maximum magnitude of the efficient power density is observed in the path's end (column 4). Corresponding values of the beam effective radius are given in column 5. For the value of the efficient power obtained, the optimum distance of focusing was determined (column 6). Columns 7 and 8 give the values of W_{ef} and R_{ef} corresponding to the optimum focusing. Column 9 presents the values of the beam diffraction radius for given focusing, which differs from the corresponding values from Table 7 (column 6) because of violating the condition $F = L$ in the latter case.

Table 8

1	2	3	4	5	6	7	8	9
Path's number	Laser number	W_{opt}, W/cm^2	W_{ef}, W/cm^2	R_{ef}, m	F_{opt}, km	W_{ef}, W/cm^2	R_{ef}, m	R_{dif}, m
1	3	23	0.65	0.73	395	0.72	0.69	0.51
2	2	22	15.4	0.63	390	18.7	0.58	0.52
2	5	370	198	1.27	370	230	1.19	0.89
3	4	230	335	0.75	240	370	0.71	0.48
4	2	38	175	0.38	260	227	0.34	0.30
5	1	11	12.5	0.35	440	14.6	0.32	0.25

The results show that in all the cases considered the optimum focusing must be sharper than the focusing in the receiving plane. This makes the obtained results qualitatively different from those for optimizing the single-frequency radiation, in which case

the optimum focusing for the paths 1, 3, and 5 is beyond the receiving plane.

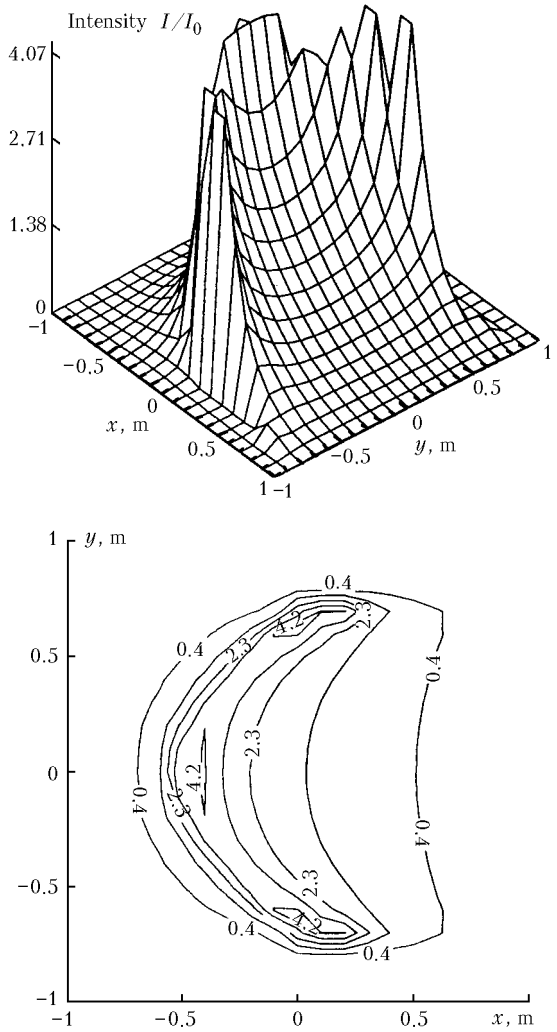

Fig. 7. Intensity distribution in the receiving plane under optimum conditions of propagation.

The calculations have shown the values of optimum power to depend on many factors and to differ by almost two orders of magnitude for the sources and paths examined. However, there is quite stable indication of the optimum for radiation propagation. Under conditions of optimum propagation (the beam power and focusing are under optimizing) the magnitude of R_{ef} exceeds by 10–50% the magnitude of the diffraction limited radius of the focusing spot corresponding to optimum focusing. In the case when only radiation power has to be optimized, R_{ef} exceeds by 50–80% the diffraction limited radius $R_{dif} = \theta_0 L$ (θ_0 is the initial angular beam divergence, L is the propagation distance) obtained in the absence of nonlinear effects. That is, the optimum conditions of propagation for different paths and radiation sources correspond to almost the same degree of beam distortion. Figure 7 presents the intensity distributions in the receiving plane for path 3 and laser 4 under optimum conditions.

Thus, as follows from the comparison of the results given in Tables 7 and 8, if R_{ef} exceeds R_{dif} by less than 10%, the initial power is essentially lower than the optimum one; the twofold and higher excess of R_{ef} over R_{dif} indicates that the initial power is essentially greater than the optimum one.

References

1. A.M. Prokhorov ed., *Reference Book on Lasers* (Sov. Radio, Moscow, 1978), Vol. 1, 504 pp.
2. N.G. Basov, V.S. Kazakevich, and I.B. Kovsh, Kvant. Elektron. **9**, No. 4, 763–771 (1982).
3. V.S. Masychev, V.G. Plotnichenko, and V.K. Sysoev, Kvant. Elektron. **8**, No. 7, 1540–1550 (1981).
4. R. Gross and J. Bott, eds., *Chemical Lasers* [Russian translation] (Mir, Moscow, 1980), 832 pp.
5. Yu.M. Andreev, S.N. Bovdey, P.P. Geiko, A.I. Gribenukov, V.A. Gurashvili, V.V. Zuev, and C.V. Izumov, Opt. Atm. **1**, No. 4, 124–127 (1988).
6. A.A. Mitsel' and K.M. Firsov, J. Quant. Spectrosc. Radiat. Transfer **54**, 549–557 (1995).
7. A.A. Mitsel', I.V. Ptashnik, K.M. Firsov, B.A. Fomin,. Atmos. Oceanic Opt. **8**, No. 10, 847–850 (1995).
8. L.S. Rothman, C.P. Rinsland, A. Goldman, S.T. Massie, D.P. Edwards, J.-M. Flaud, A. Perrin, C. Camy-Peyret, V. Dana, J.-Y. Mandin, J. Schroeder, A. Mccann, R.R. Gamache, R.B. Wattson, K. Yoshino, K.V. Chance, K.W. Jucks, L.R. Brown, V. Nemtchinov, and P. Varanasi, J. Quant. Spectrosc. Radiat. Transfer **60**, No. 6, 665–710 (1998).
9. S.A. Clough, F.X. Cneizys, and R.W. Davis, Atmos. Res. **23**, pp. 229–241 (1989).
10. V.E. Zuev, V.S. Komarov, *Statistical Models of Temperature and Gas Components of the Atmosphere* (Gidrometeoizdat, Leningrad, 1986), 264 pp.
11. D. Stroben, ed., *Propagation of Laser Beam in the Atmosphere* [Russian translation] (Mir, Moscow, 1981), 414 pp.
12. P.G. Kryukov and V.S. Letokhov, Usp. Fiz. Nauk **99**, No. 2, 169–228 (1969).
13. Yu.V. Kistenev, Izv. Vyssh. Uchebn. Zaved., Ser. Fizika **39**, No. 4, 117–122 (1996).
14. V.E. Zuev, A.A. Zemlyanov, and Yu.D. Kopytin, *Modern Problems of the Atmosphere*, Vol. 6. *Nonlinear Optics of the Atmosphere* (Gidrometeoizdat, Leningrad, 1989), 256 pp.
15. V.P. Lukin, *Atmospheric Adaptive Optics* (Nauka, Novosibirsk, 1986), 250 pp.
16. V.V. Kolosov and M.F. Kuznetsov, Atm. Opt. **2**, No. 5, 378–383 (1989).
17. A.A. Zemlyanov and S.N. Sinev, Opt. Atm. **1**, No. 1, 44–50 (1988).
18. V.A. Banakh and I.N. Smalikho, Kvant. Elektron. **14**, No. 10, 2098–2107 (1987).